

Lagrange Wavelets for Signal Processing

Zhuoer Shi, G. W. Wei, Donald J. Kouri, David K. Hoffman and Zheng Bao

MS#: 2102

Revised for IEEE Trans. Image Processing

EDICS: IP 1.6 Multiresolution Processing

ABSTRACT

This paper deals with the design of interpolating wavelets based on a variety of Lagrange functions, combined with novel signal processing techniques for digital imaging. Halfband Lagrange wavelets, B-spline Lagrange wavelets and Gaussian-Lagrange distributed approximating functional (DAF) wavelets are presented as specific examples of the generalized Lagrange wavelets. Our approach combines the perceptually dependent visual group normalization (VGN) technique and a softer logic masking (SLM) method. These are formulated to re-scale the wavelet coefficients, remove perceptual redundancy and obtain optimal visual performance for digital image processing.

***Index Terms*—Generalized Lagrange wavelets, distributed approximating functionals, visual group normalization, softer logic masking.**

This work was supported by the National Science Foundation under Grant CHE-9700297, the R.A. Welch Foundation under Grant E-0608, Department of Energy under Contract 2-7405-ENG82, the NSERC of Canada and Chinese National Science Foundation under Grant No.69572031.

Z. Shi and D. J. Kouri are with the Department of Physics, University of Houston, TX 77204, USA (e-mail: zshi@bayou.uh.edu, kouri@uh.edu).

G. W. Wei was with the Department of Physics, University of Houston, TX 77204, USA. He is now with the Department of Computational Science, National University of Singapore, Singapore 129260 (e-mail: cscweigw@nus.edu.sg).

D. K. Hoffman is with the Department of Chemistry and Ames Laboratory, Iowa State University, Ames, IA 50011, USA (e-mail: hoffman@qdynamic.ameslab.gov).

Z. Bao is with the National Key Laboratory of Radar Signal Processing, Xi'an 710071, China (e-mail: zhbao@rsp.xidian.edu.cn).

I. INTRODUCTION

The theory of interpolating wavelets has attracted much attention recently [1, 9, 11, 12, 13, 20, 21, 22, 29, 30, 33, 34, 35, 36, 37, 45, 46]. It possesses the attractive characteristic that the wavelet coefficients are obtained from the direct linear combinations of discrete samples rather than from the traditional inner product integrals. Mathematically, various interpolating wavelets can be formulated in a biorthogonal setting. Harten has described a kind of piecewise biorthogonal wavelet construction [13]. Swelden independently has developed essentially this method into the “lifting scheme” [37], which can be regarded as a special case of the Neville filters [21]. Unlike the previous method for constructing biorthogonal wavelets, which relies on explicit solution of coupled algebraic equations [5, 6, 7], the lifting scheme enables one to construct a custom-designed biorthogonal wavelet transforms assuming only a single low-pass filter without iterations. Generally speaking, the lifting-interpolating wavelet theory is closely related to: the finite element technique for the numerical solution of partial differential equations, the subdivision scheme for interpolation and approximation, multi-grid generation and surface fitting techniques. The most attractive feature of the approach is that discrete samplings are identical to wavelet multiresolution analysis. Without any pre-conditioning or post-processing that was required previously for accurate wavelet analysis, the interpolating wavelet coefficients can be implemented using a parallel computational scheme.

Lagrange interpolation polynomials are commonly used for signal approximation and smoothing. By carefully designing the interpolating Lagrange functionals, one can obtain smooth interpolating scaling functions with arbitrary order of regularity. We present three different kinds of biorthogonal interpolating Lagrange wavelets (Halfband Lagrange wavelets, B-spline Lagrange wavelets and Gaussian-Lagrange DAF wavelets) as specific examples of *generalized Lagrange wavelets*. *Halfband Lagrange wavelets* can be regarded as an extension of Dubuc interpolating functionals [9, 12], auto-correlation shell wavelet analysis [29], and halfband filters [1]. *B-spline Lagrange Wavelets* are generated by a B-spline-windowed Lagrange functional which increases the smoothness and localization properties of the simple Lagrange scaling function

and related wavelets. *Lagrange distributed approximating functionals* (LDAF)—Gaussian modulated Lagrange polynomials have been successfully applied for numerically solving various linear and nonlinear partial differential equations [45]. Typical examples include DAF-simulations of 3D reactive quantum scattering and 2D Navier-Stokes fluid flow with non-periodic boundary conditions. In terms of wavelet analysis, DAFs can be regarded as particular scaling functions (wavelet-DAFs); the associated DAF-wavelets are generated in a number of ways [34-36]. Both DAFs and DAF-wavelets are smooth and decay rapidly in both the time and frequency representations. One objective of the present work is to construct new biorthogonal DAF-wavelets and the associated DAF-filters.

As an example application of Lagrange wavelets, we consider image processing. This application requires dealing with huge data sets, complicated space-frequency distributions and complex perceptual dependent characteristics. De-noising and restoration play an important role in image processing. Noise distortion not only affects the visual quality of images, but also degrades the efficiency of data compression and coding. To exploit the time-frequency characteristics of wavelets, an earlier *group normalization* (GN) technique [31, 32] has been utilized to re-scale the wavelet coefficients. The group normalization process corrects the drawback that the coefficient magnitudes do not correctly reflect the true strength of the various signal components. In order to achieve the best noise-removing efficiency, the visual response is best accounted for by a *perceptual normalization* based on the property of the *human vision system (HVS)*. The concept of visual loss-less quantization [44] is employed to construct the visual loss-less matrix, which re-adjusts the magnitude-normalized coefficients.

Perceptual signal processing has the potential of overcoming the limits of the traditional Shannon Rate-distortion (R-D) theory for perception-dependent information, such as images and acoustic signals. Previously, Ramchandran, Vetterli, Xiong, Herley, Asai, and Orchard have utilized a rate-distortion compromise for image compression [15, 26, 27, and 47]. Our recently derived Visual Group Normalization (VGN) technique [35, 36]

can be used with rate-distortion compromise to generate a so-called *visual rate-distortion* (VR-D) theory to further improve image processing.

As an adjusted de-noising technique, *softer logic masking* (SLM) [32] is designed to improve the filtering performance of Donoho's *Soft Thresholding* method [10]. The SLM technique efficiently preserves important information (particularly at an edge transition) in a manner suited to human visual perception. In this paper, the above mentioned approaches are combined with Lagrange wavelets to achieve excellent blind image restoration performance.

II. INTERPOLATING WAVELETS

The basic characteristics of interpolating wavelets of order D require that the primary scaling functions satisfy the following conditions [11].

(1) Interpolation:

$$\phi(k) = \begin{cases} 1, & k = 0 \\ 0, & k \neq 0 \end{cases}, \quad k \in \mathbb{Z} \quad (1)$$

(2) Self-induced two-scale relation: ϕ can be represented as a linear combination of the dilates and translates of itself, while the weight is the value of ϕ at a subdivision integer of order 2.

$$\phi(x) = \sum_k \phi(k/2)\phi(2x-k) \quad (2)$$

This is only approximately satisfied for some of the interpolating wavelets discussed in the later sections; however, the approximation can be made arbitrarily accurate.

(3) Polynomial span: For an integer $D \geq 0$, the collection of formal sums, symbolized by $\sum C_k \phi(x-k)$, contains all polynomials of degree D .

(4) Regularity: For real $V > 0$, ϕ is *Hölder* continuous of order V .

(5) Localization: ϕ and all its derivatives through order $\lfloor V \rfloor$ decay rapidly.

$$|\phi^{(r)}(x)| \leq A_s (1+|x|)^{-s}, \quad x \in \mathbb{R}, s > 0, 0 \leq r \leq \lfloor V \rfloor, \quad (3)$$

here $\lfloor V \rfloor$ represents the maximum integer which does not exceed V .

■

Interpolating wavelets are particularly efficient for signal representation since their multiresolution analysis is simply realized by discrete sampling. This makes it easy to generate a subband decomposition without requiring tedious iterations. Moreover, adaptive boundary treatments and non-uniform samplings can be easily implemented using interpolating methods. Compared with commonly used wavelet transforms, the interpolating wavelet transform possesses the following characteristics:

1. The wavelet transform coefficients are generated by a linear combination of signal samplings, instead of the commonly used convolution of wavelet transform, such as

$$W_{j,k} = \int_{\mathbb{R}} \psi_{j,k}(x) f(x) dx \quad (4)$$

where $\psi_{j,k}(x) = 2^{j/2} \psi(2^j x - k)$.

2. A parallel-computing algorithm can be easily constructed. The calculation and compression of coefficients are not coupled. For the halfband filter with length L , the calculation of the wavelet coefficients does not exceed $L+2$ multiply/adds for each.
3. For a D -th order differentiable function, the wavelet coefficients decay rapidly.
4. In a minimax sense, threshold masking and quantization are nearly optimal for a wide variety of regularization algorithms.

Theoretically, interpolating wavelets are closely related to the following wavelet types:

① **Band-limit Shannon wavelets**

The π band-limited function, $\phi(x) = \sin(\pi x)/(\pi x) \in C^\infty$ in *Paley-Wiener* space, constructs interpolating functions. Every π band-limited function $f \in L^2(\mathbb{R})$ can be reconstructed by the equation

$$f(x) = \sum_k f(k) \frac{\sin \pi(x-k)}{\pi(x-k)} \quad (5)$$

where the related wavelet function (the Sinplet) is defined as (see Figure 1)

$$\psi(x) = \frac{\sin \pi(2x-1) - \sin \pi(x-1/2)}{\pi(x-1/2)} \quad (6)$$

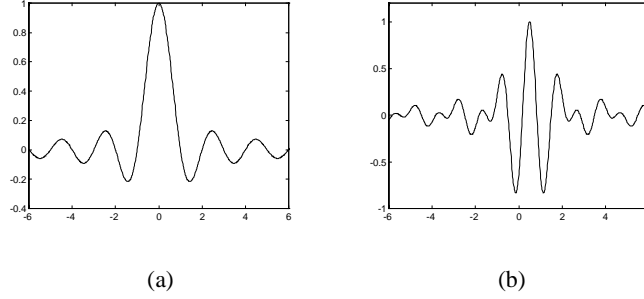


Figure 1. π band-limited interpolating wavelets. (a) *Sinc* function. (b) *Sinplet* wavelet.

② Interpolating fundamental spline

The fundamental polynomial spline of degree D , $\phi_D(x)$, where D is an odd integer, has been shown to be an interpolating wavelet (see Figure 2). It is smooth with order $R=D-1$, and its derivatives through order $D-1$ decay exponentially [39]. Thus

$$\phi_D(x) = \sum_k \alpha_D(k) \beta_D(x-k) , \quad (7)$$

where $\beta_D(x)$ is the B-spline of order D defined as

$$\beta_D(x) = \sum_{j=0}^{D+1} \frac{(-1)^j}{D!} \binom{D+1}{j} \left(x + \frac{D+1}{2} - j \right)^D U \left(x + \frac{D+1}{2} - j \right) \quad (8)$$

Here U is the step function

$$U(x) = \begin{cases} 0, & x < 0 \\ 1, & x \geq 0 \end{cases} \quad (9)$$

and $\{\alpha_D(k)\}$ is the sequence that satisfies the infinite summation condition

$$\sum_k \alpha_D(k) \beta_D(n-k) = \delta(n) \quad (10)$$

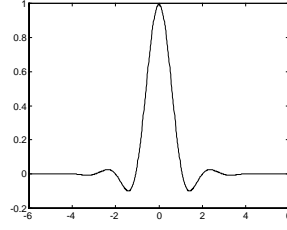


Figure 2. Interpolating Cardinal Spline ($D=5$)

③ Deslauriers-Dubuc functional

Let D be an odd integer, and $D > 0$. There exist functions, F_D , such that if F_D has already been defined at all binary rationals with denominator 2^j , it can be extended by polynomial interpolation to all binary rationals with denominator 2^{j+1} , i.e. all points halfway between previously defined points [9, 12]. Specifically, to define the function at $(k+1/2)/2^j$ when it is already defined at all $\{k2^j\}$, fit a polynomial $\pi_{j,k}$ to the data $(k'/2^j, F_D(k'/2^j))$ for $k' \in \{2^j[k-(D-1)/2], \dots, 2^j[k+(D+1)/2]\}$. This polynomial is unique

$$F_D\left(\frac{k+1/2}{2^j}\right) \equiv \pi_{j,k}\left(\frac{k+1/2}{2^j}\right) \quad (11)$$

This subdivision scheme defines a function that is uniformly continuous at the rationals and has a unique continuous extension. The function F_D is a compactly supported interval polynomial and is regular; it is the auto-correlation function of the Daubechies wavelet [8] of order $D+1$. This function is at least as smooth as the corresponding Daubechies wavelets.

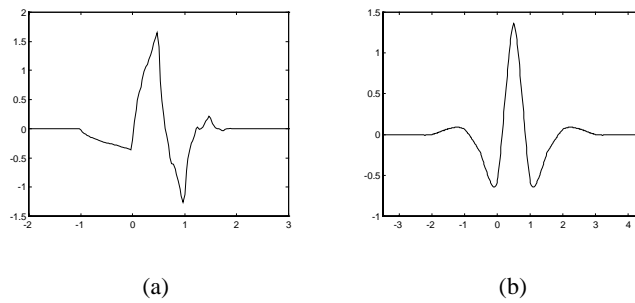


Figure 3. Interpolating wavelets by auto-correlation shell ($D=3$). (a) Daubechies wavelet. (b) Dubuc wavelet.

④ **Auto-correlation shell of orthonormal wavelets**

If $\check{\phi}$ is an orthonormal scaling function, its auto-correlation $\phi(x) = \int \check{\phi}(t)\check{\phi}(x-t)dt$ is an interpolating wavelet (Figure 3) [29]. Its smoothness, localization and two-scale relations derive from $\check{\phi}$. The auto-correlation of Haar, Larmarie-Battle, Meyer, and Daubechies wavelets lead, respectively, to the interpolating Schauder, interpolating spline, C^∞ interpolating, and Deslauriers-Dubuc wavelets.

⑤ **Lagrange half-band filters**

Ansari, Guillemot, and Kaiser [1] have used Lagrange symmetric halfband FIR filters to design the orthonormal wavelets that express the relation between the Lagrange interpolators and Daubechies wavelets. Their filter corresponds to the Deslauriers-Dubuc wavelet of order $D=7$ ($2M-1$), $M=4$. The transfer function of the halfband symmetric filter h is given by

$$H(z) = \frac{1}{2} + zT(z^2) \tag{12}$$

where T is a trigonometric polynomial. Except for $h(0)=1/2$, at every even integer lattice $h(2n)=0$, $n \neq 0, n \in Z$.

The transfer function of the symmetric FIR filter $h(n)=h(-n)$, has the form

$$H(z) = \frac{1}{2} + \sum_{n=1}^M h(2n-1)(z^{1-2n} + z^{2n-1}) \tag{13}$$

The concept of an interpolating wavelet decomposition is similar to that of “algorithm a trous”, the connection having been found by Shensa [30]. Moreover, the interpolating wavelets invoke the construction of wavelet sampling theory. Based on that, Xia et al. developed several compactly supported interpolating wavelets [46]. The self-induced scaling conditions and interpolation condition are the most important characteristics of interpolating wavelets. According to the following equation

$$f(x) = \sum_n f(n)\phi(x-n) \tag{14}$$

the signal approximation is exact on the discrete integer sampling points, which does not hold in general for commonly used non-interpolating wavelets.

III. LAGRANGE WAVELETS

A. Halfband Lagrange Wavelets

The halfband filter is defined as one whose even samples of the impulse response are constrained such that $h(0)=1/2$ and $h(2n)=0$ for $n=\pm 1, \pm 2, \dots$. A special case of symmetric halfband filters can be obtained by choosing the filter coefficients according to the Lagrange interpolation formula. The filter coefficients are then given by

$$h(2n-1) = \frac{(-1)^{n+M-1} \prod_{m=1}^{2M} (M+1/2-m)}{(M-n)!(M+n-1)!(2n-1)} \quad (15)$$

These filters have the property of maximal flatness. They possess a balance between the degree of flatness at zero frequency and flatness at the Nyquist frequency (half sampling).

These half-band filters can be utilized to generate the interpolating wavelet decomposition, which is regarded as a class of auto-correlated shells of orthogonal wavelets. The interpolating wavelet transform can also be generated by the following Lagrange polynomials [29]

$$P_{2n-1}(x) = \prod_{m=-M+1, m \neq n}^M \frac{x-(2m-1)}{(2n-1)-(2m-1)} \quad (16)$$

In such a case, the predicted interpolation is expressed as

$$\Gamma S_j(i) = \sum_{n=1}^M P_{2n-1}(0) [S_j(i+2n-1) + S_j(i-2n+1)], \quad i=2k+1, \quad (17)$$

where Γ is a projection and S_j are the low-pass coefficients at the j -th layer. This projection relation is equivalent to the subband filter response of

$$h(2n-1)=P_{2n-1}(0). \quad (18)$$

The above-mentioned interpolating wavelets can be regarded as an extension of the fundamental Deslauriers-Dubuc interactive sub-division scheme (factorized as $M=2$, while the order of Lagrange polynomial is $D=2M-1=3$) (Figure 5(a)).

It is easy to verify that an increase of the Lagrange polynomial order will introduce higher regularity in the interpolating functionals (Figure 7(a)). When $D \rightarrow +\infty$, the interpolating functional becomes the π -band-limited Sinc function and its definition domain is the real line. The subband filters generated by Lagrange interpolating functionals satisfy

- (1) Interpolation: $h(\omega) + h(\omega + \pi) = 1$.
- (2) Symmetry: $h(\omega) = h(-\omega)$.
- (3) Vanishing Moments: $\int_{\mathbb{R}} x^p \phi(x) dx = \delta_p$.

Donoho outlines a basic subband extension for perfect reconstruction. He defines the wavelet function as

$$\psi(x) = \phi(2x-1) \tag{19}$$

The biorthogonal subband filters are expressed as

$$\tilde{h}(\omega) = 1, \quad g(\omega) = e^{-i\omega}, \quad \tilde{g}(\omega) = e^{-i\omega} \overline{h(\omega + \pi)} \tag{20}$$

However, the Donoho interpolating wavelets have some drawbacks, because the low-pass coefficients are generated by a sampling operation only. As the decomposition layer increases, the correlation between low-pass coefficients becomes weaker. The interpolating (prediction) error (high-pass coefficients) strongly increases, which destroys the compact representation of the signal. Additionally, it does not lead to a Riesz basis for $L^2(\mathbb{R})$ space.

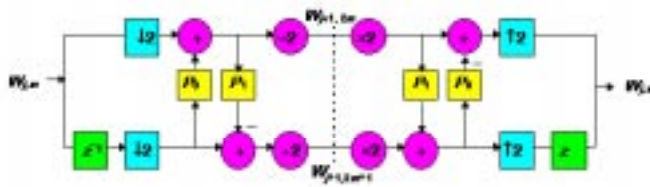


Figure 4. Lifting scheme.

Swelden has provided, by far, the most efficient and robust scheme [37] for constructing biorthogonal wavelet filters. His approach is to generate high-order interpolating Lagrange wavelets with increased regularity. As Figure 4 shows, P_0 is the interpolating prediction process, and P_1 the updating filter, makes the down-sampling low-pass coefficients smoother. A simple example is to choose P_0 be the same as P_1 . In this case, the interpolating subband filters are

$$\begin{cases} h_1(\omega) = h(\omega) \\ \tilde{h}_1(\omega) = 1 + \tilde{g}(\omega)\overline{P(2\omega)} \\ g_1(\omega) = e^{-i\omega} - h(\omega)P(2\omega) \\ \tilde{g}_1(\omega) = \tilde{g}(\omega) \end{cases} \quad (21)$$

The newly developed filters h_1 , g_1 , \tilde{h}_1 , and \tilde{g}_1 also construct the biorthogonal dual pair for perfect reconstruction. Examples of generated biorthogonal lifting wavelets (with different regularity) and the associated equivalent subband filter responses are shown in Figure 5-8.

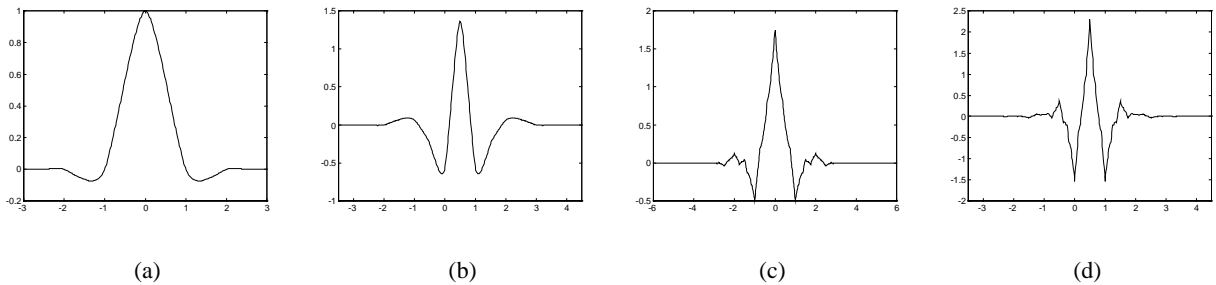


Figure 5. Lagrange Wavelets with $D=3$. (a) Scaling. (b) Wavelet. (c) Dual scaling. (d) Dual wavelet.

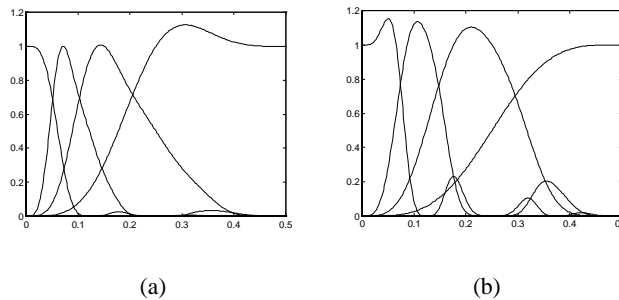


Figure 6. Frequency response of equivalent filters ($D=3, J=3$). (a) Decomposition. (b) Reconstruction.

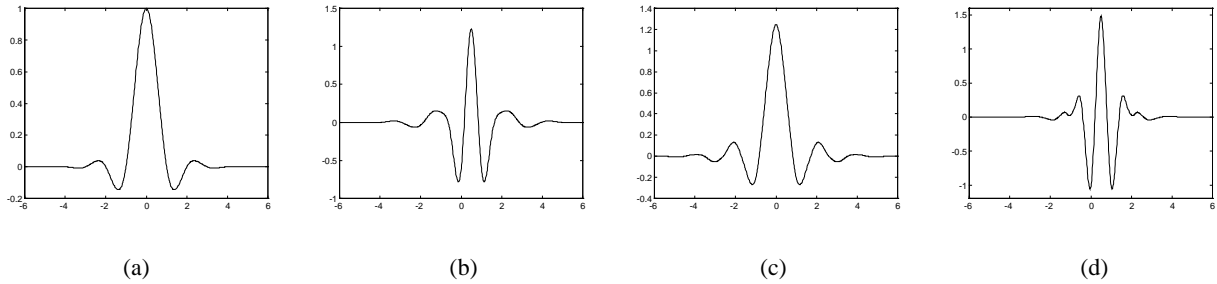


Figure 7. Lagrange wavelets with $D=9$. (a) Scaling. (b) Wavelet. (c) Dual scaling. (d) Dual wavelet.

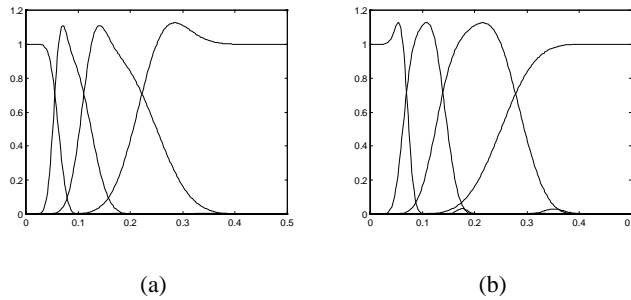
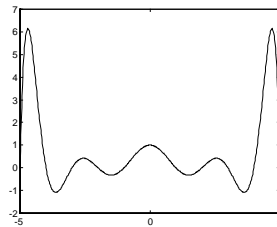


Figure 8. Frequency response of equivalent filters ($D=9, J=3$). (a) Decomposition. (b) Reconstruction.

B. B-Spline Lagrange Wavelets

Lagrange polynomials are the natural interpolating expressions. Utilizing a different expression for the Lagrange polynomials, we construct the extension of interpolating wavelets.



(a)

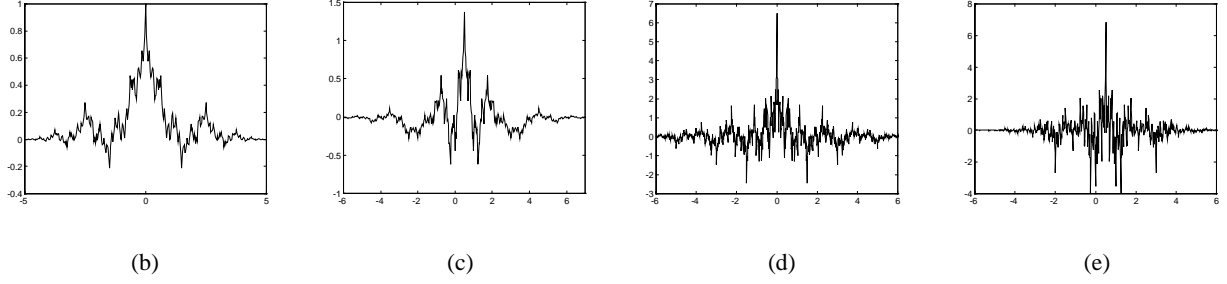


Figure 9. Non-regularized Lagrange wavelets ($M=5$). (a) Lagrange polynomial. (b) Scaling. (c) Wavelet. (d) Dual scaling. (e) Dual wavelet.

If we define a class of symmetric Lagrange interpolating functional shells as

$$P_M(x) = \prod_{i=-M, i \neq 0}^M \frac{x-i}{-i}, \quad (22)$$

it is easy to verify that this Lagrange shell also satisfies the interpolating condition on discrete integer points, since

$$P_M(k) = \begin{cases} 1, & k = 0 \\ 0, & \text{otherwise} \end{cases} \quad (23)$$

However, simply defining the filter response as

$$h(k) = \frac{1}{2} P\left(\frac{k}{2}\right), \quad k=-M, M \quad (24)$$

will lead to the non-stable interpolating wavelets, as shown in Figure 9.

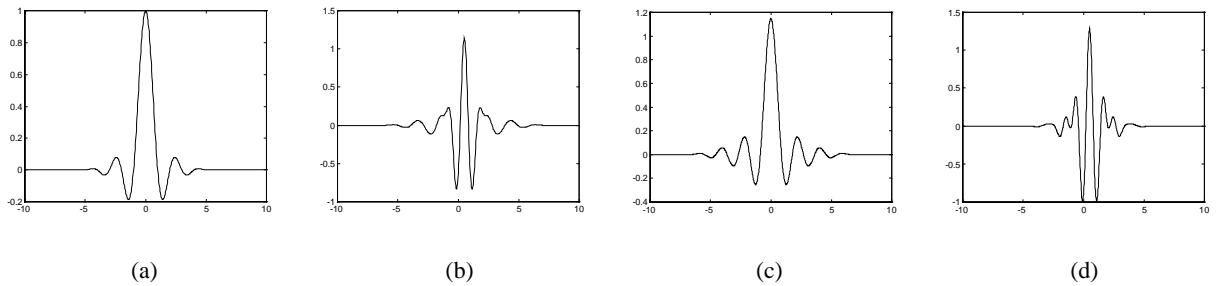


Figure 10. B-Spline Lagrange DAF wavelets ($D=4, \eta=2$). (a) Scaling. (b) Wavelet. (c) Dual scaling. (d) Dual wavelet.

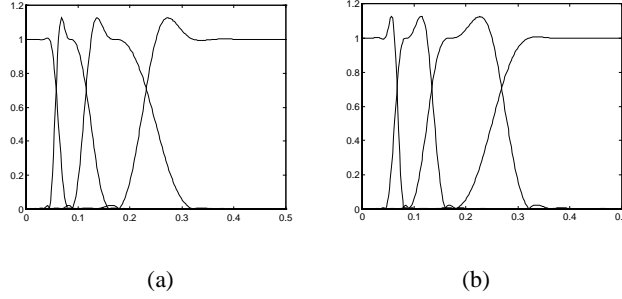


Figure 11. Frequency Response of Equivalent Filters ($D=4$, $\tau=2$). (a) Decomposition. (b) Reconstruction.

Utilizing a smooth window, which vanishes at the zeros of the Lagrange polynomial, makes more regular interpolating wavelets and equivalent subband filters (as in Figs. 10 and 11). If we select a well-defined B-spline function as the weight window, then the scaling function (mother wavelet) will become an interpolating B-Spline Lagrange functional (BSLF) as

$$\begin{aligned}\phi_{M,\tau}(x) &= \frac{\beta_D(x/\tau)}{\beta_D(0)} P_M(x), \\ &= \frac{\beta_D(x/\tau)}{\beta_D(0)} \prod_{i=-M, i \neq 0}^M \frac{x-i}{-i},\end{aligned}\quad (25)$$

where D is the B-spline order, and τ is the scaling factor to control the window width. To ensure coincidence of the zeroes of the B-spline and the Lagrange polynomial, we set

$$2M=(N+1)\tau \quad (26)$$

To preserve the interpolation condition, the B-spline envelope factor M should be an odd number. It is easy to show that when the B-spline order is $D=4k+1$, τ can be any odd integer ($2k+1$). If D is an even integer, then τ can only be 2. When $D=4k-1$, we cannot construct an ideal interpolating shell according to the above definition. From the interpolation and self-induced scaling of the interpolating wavelets, it is easy to establish the subband filter response

$$h(k) = \frac{1}{2} \phi_M\left(\frac{k}{2}\right), \quad k=-2M+1, 2M-1, \quad (27)$$

C. Gaussian-Lagrange DAF Wavelets

The Gaussian Lagrange distributed approximating functional (GLDAF) can also be used as a basic scaling function to construct interpolating wavelets. These are

$$\begin{aligned}\phi_{M,\sigma}(x) &= W_\sigma(x)P_M(x) \\ &= W_\sigma(x) \prod_{i=-M, i \neq 0}^M \frac{x-i}{-i}\end{aligned}\tag{28}$$

where $W_\sigma(x)$ is a window function which is selected to be a Gaussian,

$$W_\sigma(x) = e^{-x^2/2\sigma^2},\tag{29}$$

because it satisfies the minimum frame bound condition in quantum physics. Here σ is a window width parameter, and $P_M(x)$ is the Lagrange interpolation kernel. The DAF scaling function has been successfully introduced as the basis for an efficient and powerful grid method for quantum dynamical propagation [45]. Using the lifting scheme, a wavelet basis is generated. The Gaussian window in our DAF-wavelets efficiently smoothes out the Gibbs oscillations, which plague most conventional wavelet bases. The following equation shows the close connection between the B-spline function and the Gaussian window [39]:

$$\beta_D(x) \cong \sqrt{\frac{6}{\pi(D+1)}} \exp\left(\frac{-6x^2}{D+1}\right)\tag{30}$$

for large D . As in Figure 12, if we choose the window width to be

$$\sigma = \tau\sqrt{(D+1)/12},\tag{31}$$

the Gaussian Lagrange wavelets are similar to the B-spline Lagrange wavelets. Usually, the Gaussian Lagrange DAF based wavelets are smoother and decay more rapidly than B-spline Lagrange wavelets as shown in Figure 12. If we select more sophisticated window shapes, the Lagrange wavelets can be generalized further. We shall call these extensions Bell-windowed Lagrange wavelets. The above-mentioned interpolating wavelet construction using the Lagrange polynomials can be extended to produce arbitrary customer-designed wavelets using any continuous smooth functionals. The details are studied in our further papers.

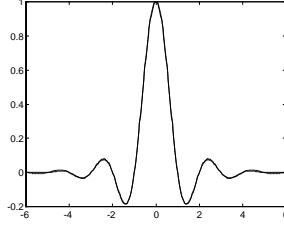


Figure 12. Mother wavelet comparison ($D=4$, $\tau=2$). Solid: B-spline Lagrange; dotted: Gaussian Lagrange

IV. VISUAL GROUP NORMALIZATION

It is well known that the mathematical theory of wavelet transforms and associated multiresolution analyses has applications in signal processing and engineering problems, where appropriate subband filters are the central entities. The goal of wavelet signal filtering is to preserve meaningful signal components, while efficiently reducing noise components. To this end, we use known magnitude normalization techniques [31, 32] and develop a new perceptual normalization to account for the human vision response.

From a signal processing point of view, wavelet coefficients can be regarded as the results of the signal passing through an *equivalent decomposition filter* (EDF). The responses of the EDF $LC_{j,m}(\omega)$ are the combination of several recurrent subband filters at different stages. As shown in Figure 6., the EDF amplitudes of different sub-blocks are different. Thus the magnitude of the decomposition coefficients in each of the sub-blocks will not exactly reproduce the true strength of the signal components. Stated differently, various EDFs are incompatible with each other in the wavelet transform. To adjust the magnitude of the response in each block, the decomposition coefficients are re-scaled with respect to a common magnitude standard. Thus the EDF coefficients $C_{j,m}(k)$ on layer j and block m should be multiplied by a magnitude normalized factor, $\lambda_{j,m}$, to obtain an adjusted magnitude representation. This factor is chosen as the reciprocal of the maximum magnitude of the frequency response of the equivalent filter on node (j,m)

$$\lambda_{j,m} = \frac{1}{\sup_{\omega \in \Omega} \{|LC_{j,m}(\omega)|\}} \quad \Omega = [0, 2\pi] \quad (32)$$

This idea was recently extended to *group normalization* (GN) of wavelet packets for signal processing [31, 32].

An image can be regarded as the result of a real object processed by a human visual system. The latter has essentially many subband filters. The responses of these human filters to various frequency distributions are not at all uniform. Therefore, an appropriate alteration of the wavelet coefficients is necessary. Actually, the human visual system is adaptive and has variable lens and focuses for different visual environments. Using a just-noticeable distortion profile, we can efficiently remove the visual redundancy from decomposition coefficients and normalize them with respect to a standard of perception importance. A practical, simple model for perception efficiency has been presented by Watson, et al. [44] for data compression. This model is adapted here to construct the “perceptual lossless” response magnitude $Y_{j,m}$ for normalizing according to the visual response function,

$$Y_{j,m} = a10^{k \left(\log \frac{2^j f_0 d_m}{R} \right)^2}, \quad (33)$$

where a defines the minimum threshold, k is a constant, R is the Display Visual Resolution (DVR), f_0 is the spatial frequency, and d_m is the directional response factor. The generation of $Y_{j,m}$ can be found in [44]. Together with the magnitude normalized factor $\lambda_{j,m}$, this induces the perceptual lossless quantization matrix as

$$Q_{j,m} = 2Y_{j,m}\lambda_{j,m} \quad (34)$$

This treatment provides a simple, human-vision-based threshold technique for the restoration of the most important perceptual information in an image. We refer to the combination of the above mentioned two normalizations as the *visual group normalization* (VGN) of wavelet coefficients. Note here that we use λ_m for magnitude normalization and not the wavelet “basis function amplitude” in [44], because the digital image decomposition is completely done using filter banks.

V. MASKING TECHNIQUE

5.1. Hard Logic Masking

The VGN provides an efficient approach for re-normalizing the wavelet decomposition coefficients so that various subband filters have appropriate perceptual impulse responses. However, this algorithm alone does not yield the best SNR in real signal processing. Essentially, various noise and/or interference components are embedded in each node of the subband decomposition tree. To achieve SNR-improved reconstruction of the signal and/or image, a filtering process is needed to reduce the noise and preserve the important signal information. Noise due to random processes has a comparatively wide-band distribution over the decomposition tree, whereas mechanical noise may have a narrow-band distribution over a few specific subband components. Therefore, time-varying masking techniques are utilized to reduce noise. We discuss a few useful masking methods in the rest of this subsection.

Single Dead-Zone Threshold Masking

With a given decomposition tree, a constant threshold r is selected for our magnitude normalized wavelet decomposition coefficients $NC_{j,m}(k)$. That is, if the absolute value of $NC_{j,m}(k)$ is greater than the threshold r , the original decomposition coefficient is kept; otherwise it is set to zero. That is

$$C_{j,m}(k) = \begin{cases} C_{j,m}(k) & |NC_{j,m}(k)| > r \\ 0 & |NC_{j,m}(k)| < r \end{cases} \quad (35)$$

This approach is similar to the *pass-band selection* technique [48], used in a FFT framework. However, in the present approach, the decomposition coefficients are re-scaled using the visual group normalization. Therefore, even with a single zone masking, it is expected that for a given noisy signal the present wavelet analysis will achieve a better SNR than that of a single-band FFT method.

Adaptive Node Mean/Variance Threshold Masking

In practice, we hope the threshold r can be adaptively adjusted to the strength of the noisy environment. Thus the threshold r should be set higher to suppress a noisier signal, and in general, r should vary as a function of the statistical properties of the wavelet decomposition coefficients, the simplest and most important of which are the mean and second variance. These are incorporated in the present work.

We define the mean and second variance of the magnitude of the normalized coefficients on node (j,m) as

$$\eta_{j,m} = \frac{1}{N_j} \sum_{k=0}^{N_j-1} NC_{j,m}(k) \quad (36)$$

and

$$\sigma_{j,m} = \left(\frac{1}{N_j} \sum_{k=0}^{N_j-1} [NC_{j,m}(k) - \eta_{j,m}]^2 \right)^{\frac{1}{2}}, \quad (37)$$

where $N_j=2^jN$ and N is the total length of the signal. A masking is then set according to the following analysis:

(1) Introduce a factor $|\alpha|<1$, $\alpha \in R$. (2) If $\alpha|NC_{j,m}(k)-\eta_{j,m}|<\sigma_{j,m}$, it implies that the normalized coefficient $NC_{j,m}(k)$ is near the mean value $\eta_{j,m}$ on node (j,m) , and the variance $\sigma_{j,m}$ is greater. Then $NC_{j,m}(k)$ is regarded as a noise or clutter component, and the correspondent original WPT coefficient $C_{j,m}(k)$ is set to zero. (3) If $\alpha|NC_{j,m}(k)-\eta_{j,m}| \geq \sigma_{j,m}$, it implies that $NC_{j,m}(k)$ is far from the mean value $\eta_{j,m}$ and the variance $\sigma_{j,m}$ is smaller, the interference is weak. $NC_{j,m}(k)$ is determined as a target component, and the coefficients $C_{j,m}(k)$ is retained. The rules are summarized as

$$C_{j,m}(k) = \begin{cases} C_{j,m}(k), & \alpha | NC_{j,m}(k) - \eta_{j,m} | \geq \sigma_{j,m} \\ 0, & \alpha | NC_{j,m}(k) - \eta_{j,m} | < \sigma_{j,m} \end{cases}. \quad (38)$$

Adaptive Whole Tree Threshold Masking

For certain applications, it is possible that all $NC_{j,m}(k)$ on a particular node (j,m) have essentially the same values. The aforementioned adaptive node mean/variance threshold masking technique becomes invalid in such a case. We use an adaptive whole-tree threshold masking method for this situation. The basic procedure

is very similar to the node-based processing, except that the mean and second variance are calculated for the whole tree T , according to

$$\eta = \frac{1}{N} \sum_j \sum_m \sum_{k=0}^{N_j-1} NC_{j,m}(k) \quad (39)$$

and

$$\sigma = \left(\frac{1}{N} \sum_j \sum_m \sum_{k=0}^{N_j-1} [NC_{j,m}(k) - \eta]^2 \right)^{\frac{1}{2}}, \quad (j,m) \in T. \quad (40)$$

The corresponding reconstruction coefficients are selected by the rules

$$C_{j,m}(k) = \begin{cases} C_{j,m}(k), & \alpha | NC_{j,m}(k) - \eta | \geq \sigma \\ 0, & \alpha | NC_{j,m}(k) - \eta | < \sigma \end{cases} \quad (41)$$

Constant False Alarm Masking

In certain applications, such as radar signals generated from a given environment, it is useful to select an alarm threshold r based on the mean value of multiple measurements of the background signal. This approach is similar to a background-contrasted signal processing in which only the differences of the signal's optimal tree decomposition coefficients $NC_{j,m}(k)$ and the background decomposition coefficients $NB_{j,m}(k)$ of the same tree structure, are used for background-contrasted signal reconstruction.

5.2. Softer Logic Masking

The various maskings discussed above can be regarded as *hard logic masking*, which are similar to a bias-estimated *dead-zone limiter*. Jain [16] has shown that a non-linear dead-zone limiter can improve the SNR for weak signal detection

$$\eta(y) = \text{sgn}(y) \left(|y| - \delta \right)_+^\beta, \quad -1 \leq \beta \leq 1, \quad (42)$$

where δ is a threshold value. The positive function $(x)_+$ is defined as

$$(x)_+ = \max\{x, 0\} \quad (43)$$

Donoho has shown that the $\beta=1$ case of the above expression is a nearly optimal estimator for adaptive NMR data smoothing and de-noising [10]. Independently, two of the present authors (Shi and Bao) in a previous work [31, 32] have utilized hard logic masking to extract a target from formidable background noise efficiently.

The various threshold cutoffs of multiband expansion coefficients in hard logic masking methods are very similar to the cutoff of a FFT expansion. Thus, Gibbs oscillations associated with FFTs will also occur in the wavelet transform using a hard logic masking. Although hard logic masking methods with appropriate threshold values do not seriously change the magnitude of a signal after reconstruction, they can cause considerable edge distortions in a signal due to the interference of additional high frequency components induced by the cutoff. The higher the threshold value, the larger the Gibbs oscillation will be. Since image edges are especially important in visual perception, hard logic masking can only be used for weak noise signal (or image) processing (such as electrocardiogram (ECG) signal filtering), where relatively small threshold values are required. In this paper, we propose a *soft logic masking* (SLM) method. In our SLM approach, a smooth transition band near each masking threshold is introduced so that any decomposition coefficients, which are smaller than the threshold value is reduced gradually to zero, rather than being exactly *set* to zero. This treatment efficiently suppresses the edge oscillations and preserves image edges, and consequently improves the resolution of the reconstructed image. The SLM method is expressed as

$$\hat{C}_{j,m}(k) = \text{sgn}[C_{j,m}(k)] \times [|C_{j,m}(k)| - \delta]_+^\beta \times S[\overline{NC}_{j,m}(k)] \quad (44)$$

where $\hat{C}_{j,m}(k)$ are the decomposition coefficients to be retained in the reconstruction and quantity $\overline{NC}_{j,m}(k)$ is defined as

$$\overline{NC}_{j,m}(k) = \frac{|NC_{j,m}(k)|}{\max_{(j,m) \in T} \{|NC_{j,m}(k)|\}}. \quad (45)$$

The softer logic window mapping, $S:[0,1] \rightarrow [0,1]$, is a non-linear, monotonically increasing sigmoid functional. It is interesting to know that Nowak has also designed an alternative nonlinearity solution independently to improve the Donoho thresholding [25]. The Nowak nonlinear shrinkage functional is as

$$\eta(y) = y\Lambda(y) \quad , \quad (46)$$

where the nonlinear window function Λ is defined as

$$\Lambda(y) = \left(\frac{y^2 - \delta^2}{y^2 + \frac{\delta^2}{N-1}} \right)_+ \quad , \quad (47)$$

and N is the signal size. A comparison of the hard logic, Nowak, and softer logic masking windows is depicted in Figure 13. Our masking window is a dual-side infinitely smooth functional near threshold with maximum flat response both in dead-zone and pass band, the Nowak window is only a right-side smooth function around the threshold with less flat pass-band. Donoho's window is a non-smooth signum solution.

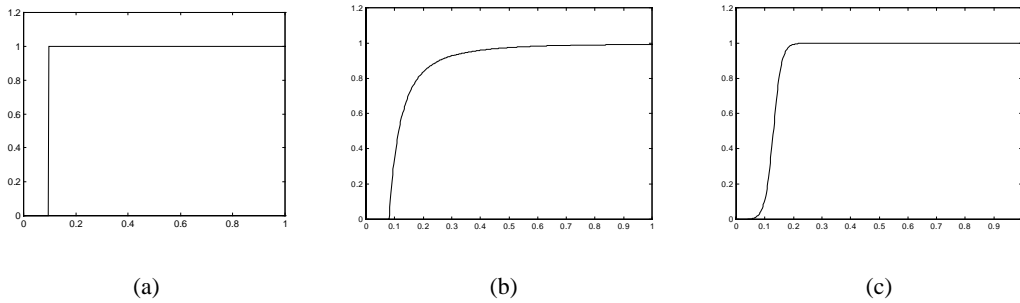


Figure 13. Nonlinear masking windows. (a) Donoho window. (b) Nowak window. (c) SLM window.

In 2D image processing, it is often important to preserve the image gradient along the xy -direction. For this purpose, we modify the aforementioned softer logic functional to

$$\hat{C}_{j,m}(k) = C_{j,m}(k) S \left(\frac{NC_{j,m}(k) - \zeta}{1 - \zeta} \right) \quad , \quad (48)$$

where ζ is a normalized adaptive threshold. For an unknown noise level, a useful approximation to ζ is given by

$$\zeta = \gamma_{upper} \hat{\sigma} \sqrt{2 \log N / N}, \quad (49)$$

where $\hat{\sigma}$ is a scaling factor conveniently chosen as $\hat{\sigma} = 1/1.349$. The quantity γ_{upper} is an upper frame boundary of the normalized wavelet transform, i.e. the upper boundary singular value of the normalized wavelet decomposition matrix. Using arguments similar to those given by Donoho [10], one can show that the above Softer Logic Masking reconstruction is a nearly optimal approximation in the minimax error sense.

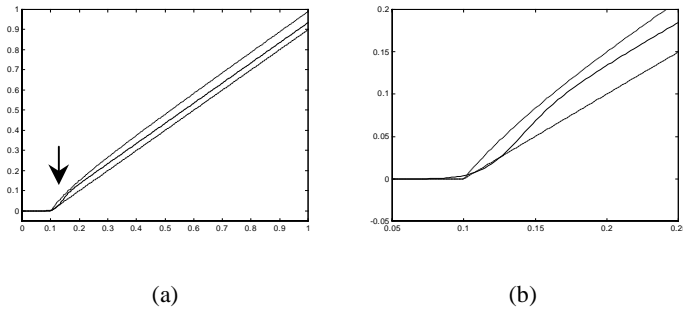


Figure 14. Comparison of the nonlinear filtering. (a) Original. (b) Enlargement around threshold area.

(Dashed line—Donoho filter; Dotted line—Nowak filter; Solid line—SLM filter)

The resulting nonlinear shrinkage filters η are compared in Figure 14. As shown in the enlarged local area around the threshold, our softer logic masking shrinkage (the solid line in the middle) expresses the optimal feature of smoothness.

VI. EXPERIMENTAL RESULTS

Generally, the possible image noise sources include photoelectric exchange, photo spots, the error of image communication, etc. The noise causes the visual perception to generate speckles, blips, ripples, bumps, ringings and aliasing. The noise distortion not only affects the visual quality of the images, but also degrades

the efficiency of data compression and coding. The traditional image processing techniques can be classified as two kinds: linear or non-linear. The principle methods of linear processing are local averaging, low-pass filtering, band-limit filtering or multi-frame averaging. Local averaging and low-pass filtering only preserve the low band frequency components of the image. The original pixel strength is substituted by an average of its neighboring pixels (within a square window). The mean error may be improved but the averaging process blurs the silhouette and finer details of the image. Band-limited filters are utilized to remove the regularly appearing dot matrix, texture and skew lines. They are useless for noise whose correlation is weak. Multi-frame averaging requires that the images be still, and the noise distribution stationary. These conditions are violated for motion picture images or for a space (time)-varying noisy background.

The traditional image quality is characterized by a mean square error (*MSE*), which possesses the advantage of a simple mathematical structure. For a discrete signal $\{s(n)\}$ and its approximation $\{\hat{s}(n)\}$, $n=0, \dots, N$, the *MSE* is defined to be

$$MSE = \frac{1}{N} \sum_{n=0}^{N-1} [\hat{s}(n) - s(n)]^2 \quad (50)$$

However, the *MSE* based evaluation standard, (such as $PSNR = \log[(255 \times 255) / MSE]$), can not exactly evaluate the image quality unless one neglects the effect of human perception. The minimum *MSE* rule causes strong undulations of the image level and destroys the smooth transition information around the pixels. Modified regularization methods may degrade the image resolution.

Generally, unsatisfactory traditional image processing is always defined on the whole space (time) region, which does not localize the space (time)-frequency details of the signal. New theoretical research shows that non-Gaussian and non-stationary characteristics are important components in human visual response. Human visual perception is more sensitive to image edges which consist of sharp-changes of the neighboring luminance because it is essentially adaptive and has variable lens and focuses for different visual environments. To protect edge information as well as remove noise, modern image processing techniques are

predominantly based on non-linear methods. Before the smoothing process, the image edges, as well as perceptually sensitive texture must be detected. The commonly used non-linear filtering approaches include median filtering, and weighting average, etc. Median filtering uses the median value within the window instead of the original value of the pixel. This method causes less degradation for slanted functions or square functions, but suppresses the signal impulses, which are shorter than half of the window length. This will degrade the image quality. The most serious shortcomings of weighting average method are that the weighting-window is not adaptive, and large-scale, complicated calculations are required to generate pixel values. If the window is made wider, more details will be removed.

The efficient HVS-based image processing techniques possess the advantages of 1) large range de-correlation for convenience of compression and filtering; 2) high perceptual sensitivity and robustness; 3) filtering according to human visual response. It therefore can enhance the most important visual information, such as edges, while suppressing the large scale of flat regions and background. In addition 4) it can be carried out with real-time processing.

The space (time)-scale logarithmic response characteristic of the wavelet transform is similar to the HVS response. Visual perception is sensitive to narrow band low-pass components, and is insensitive to wide band high frequency components. Moreover, from research in neurophysiology and psychophysical studies, the direction-selective cortex filtering is very much like 2D-wavelet decomposition. The high-pass coefficients of the wavelet transform can be regarded as the visible difference predictor (VDP).

Utilizing the modified wavelet analysis-VGN wavelet transform presented in this paper, we correct the drawback that the raw magnitudes of the transform coefficients do not exactly yield the perceptual strength of digital images. The non-linear SLM filtering provides edge-preservation for images, which removes the haziness encountered with commonly used filtering techniques.

To test our approaches, the benchmark 512×512 Y-component images are employed. The first test is for the so-called “Lena” image, which possesses clear sharp edges, strong contrast and brightness. The second picture

tested is “Barbara”. The variety of texture components and consequently high frequency edges in the Barbara image create considerable difficulties for commonly used filtering techniques. We choose 2D LDAF wavelets as the testing analysis tools for image processing. The four 2D wavelets are shown in Figure 15.

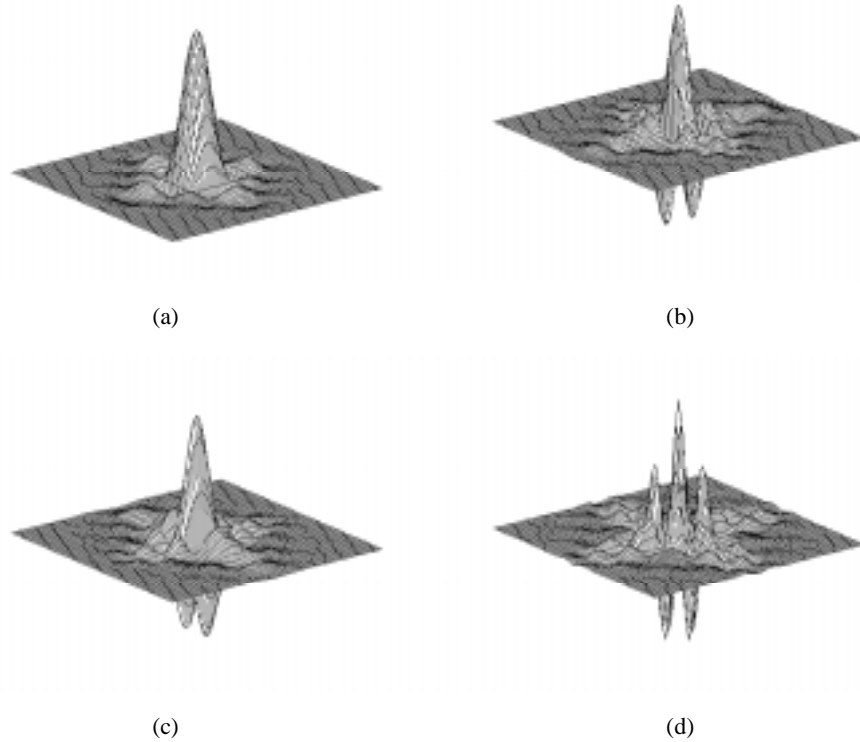


Figure 15. Lagrange wavelets for image processing. (a) Scaling. (b) Vertical. (c) Horizontal. (d) Diagonal wavelets.

The popular B97 wavelets [7, 43] are used in comparison with the generalized Lagrange wavelet technique. As shown in Figure 16, both LDAF wavelets and their dual partners display excellent smoothness and rapid decay compared with the B97 wavelets (Figure 17). The Gaussian window efficiently smoothes out the fractal-like oscillations, which plague many wavelets. The EDF responses of both the DAF and B97 wavelets are shown in Figure 18. It is obviously that the DAF’s possess smaller sidelobes, and therefore lead to less frequency leakage distortion.

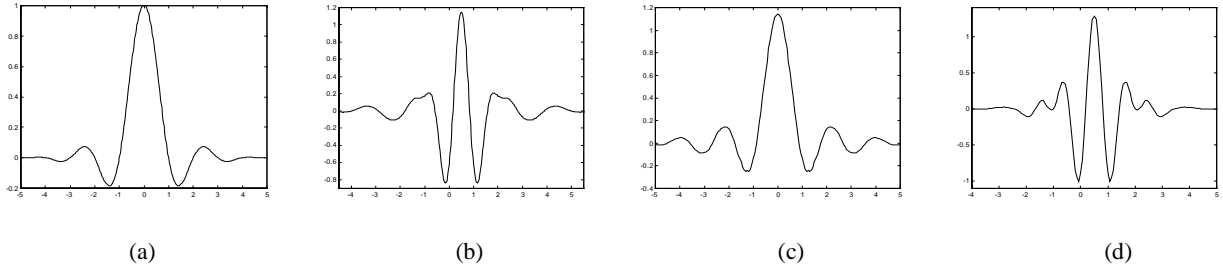


Figure 16. LDAF wavelets. (a) Scaling. (b) Wavelet. (c) Dual scaling. (d) Dual wavelet.

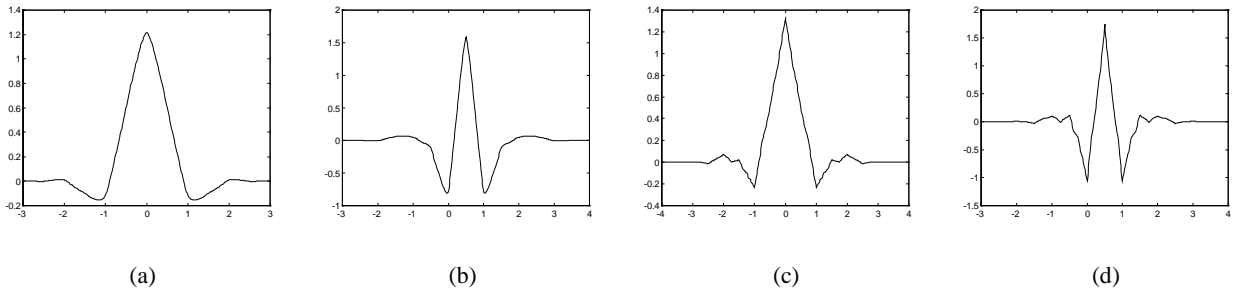


Figure 17. B97 wavelets. (a) Scaling. (b) Wavelet. (c) Dual scaling. (d) Dual wavelet.

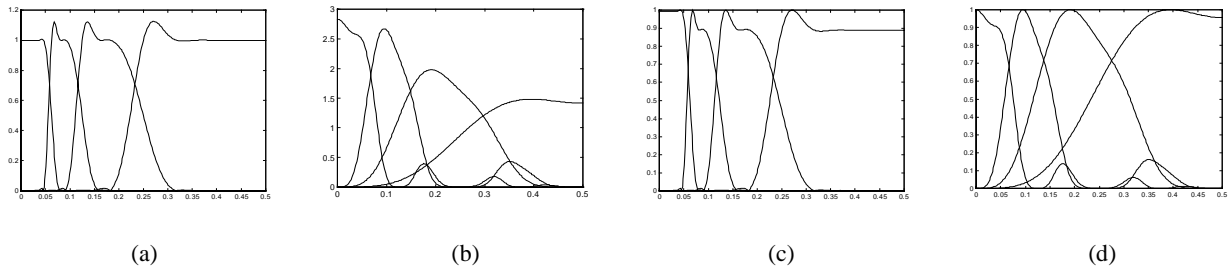


Figure 18. Frequency response of equivalent filters. (a) Non-normalized response (GLDAF). (b) Non-normalized response (B97). (c) Normalized response (GLDAF). (d) Normalized response (B97).

As shown in Figure 19(a) and (c) respectively, additive Gaussian random noise degrades the original Lena and Barbara images. The PSNR results of B97 filtering, B97 VGN filtering and LDAF wavelet processing are compared in Table I, while the perceptual quality of the GLDAF-VGN processed Lena and Barbara are shown in Figure 19(b) and (d). It is evident that our VGN wavelet technique yields optimal PSNR, better contrast and edge-preservation results, as well as provides high quality visual performance.

Table 1. Performance comparison by PSNR (dB)

Noisy Images		Median	B97 (Non-VGN)	B97 (VGN)	GLDAF (VGN)
Barbara	17.60	22.01	22.81	24.27	24.63
	20.30	23.23	24.15	25.67	26.19
	24.50	24.39	27.01	28.38	29.03
Lena	16.46	26.23	23.38	26.74	27.30
	20.07	27.40	25.71	28.51	28.96
	24.47	28.41	28.18	30.98	31.43



(a)



(b)



(c)



(d)

Figure 19. VGN processing. (a) Noisy Lena (PSNR=24.47dB). (b) Our restoration (PSNR=31.43).

(c) Noisy Barbara (PSNR=24.50dB). (d) Our restoration (PSNR=29.03).

VII. CONCLUSIONS

This paper discusses the design of interpolating wavelets based on Lagrange functions and their application in image processing. The most attractive property of the interpolating wavelets is that the wavelet multiresolution analysis is realized by discrete sampling. Thus pre- and post-conditioning processings are not needed for an accurate wavelet analysis. The wavelet coefficients are obtained from linear combinations of sample values rather than from integrals, which implies the possibility of using parallel computation techniques. Theoretically, our approach is closely related to the finite element technique for the numerical solution of partial differential equations, the subdivision scheme for interpolation approximations, multi-grid methods and surface fitting techniques. In this paper, we generalize the definition of interpolating Lagrange wavelets and produce three different biorthogonal interpolating Lagrange wavelets, namely Halfband Lagrange wavelets, B-spline Lagrange wavelets and Gaussian-Lagrange DAF wavelets.

Halfband Lagrange wavelets can be regarded as an extension of Dubuc interpolating functionals, auto-correlation shell wavelet analysis and halfband filters. B-spline Lagrange Wavelets are generated by B-spline windowing of a Lagrange functional, and lead to increased smoothness and localization compared to the basic Lagrange wavelets. *Lagrange distributed approximating functionals* (LDAF) are taken to be scaling functions (wavelet-DAFs). DAFs are smoothly decaying in both time and frequency representations. The present work extends the DAF approach to signal and image processing by constructing new biorthogonal DAF-wavelets and associated DAF-filters using a lifting scheme.

For image processing applications, we combine two important techniques, the coefficient normalization method and perceptual lossless quantization based on *human vision systems* (HVS). The resulting combined technique is called *visual group normalization* (VGN) processing [31]. The concept of *visual lossless quantization* (VLQ) leads to a potential breakthrough compared to the traditional Shannon rate-distortion theory in perception-based information processing. A modified version of Donoho's soft thresholding for image restoration, termed the *softer logic perceptual masking* (SLM) technique, is given for dealing with

extremely noisy backgrounds. This technique better preserves the important visual edges and contrast transition portions of an image and is readily adaptable to human vision. Computational results show that our Lagrange wavelet based VGN processing is extremely efficient and robust for digital image blind restoration and yields the optimal performance.

REFERENCES

- [1] R. Ansari, C. Guillemot, and J. F. Kaiser, "Wavelet construction using Lagrange halfband filters," *IEEE Trans. CAS*, vol.38, no.9, pp.1116-1118, 1991.
- [2] R. Baraniuk, D. Jones, "Signal-dependent time-frequency analysis using a radially Gaussian kernel," *Signal Processing*, Vol.32, pp.263-284, 1993.
- [3] C. M. Brislawn, "Preservation of subband symmetry in multirate signal coding," *IEEE Trans. SP*, vol.43, no.12, pp.3046-3050, 1995.
- [4] H. A. Chipman, E. D. Kolaczyk, R. E. McCulloch, "Adaptive Bayesian wavelet shrinkage," *J. American Statistical Association*, vol. 92, No. 440, pp.1413-1421, 1997.
- [5] C. K. Chui, *An Introduction to Wavelets*, Academic Press, New York, 1992.
- [6] C. K. Chui, *Wavelets: A Tutorial in Wavelet Theory and Applications*, Academic Press, New York, 1992.
- [7] A. Cohen, I. Daubechies, and J.C. Feauveau, "Biorthogonal bases of compactly supported wavelets," *Comm. Pure & Appl. Math* 45, pp. 485--560, 1992.
- [8] I. Daubechies, "Orthonormal bases of compactly supported wavelets", *Comm. Pure and App. Mathematics*, vol.41, no.11, pp.909~996, 1988.
- [9] G. Deslauriers, S. Dubuc, "Symmetric iterative interpolation processes," *Constructive Approximations*, vol. 5, pp.49-68, 1989.
- [10] D. L. Donoho, "De-noising by soft-threshold," *IEEE Trans. Inform. Theory*, vol. 41, no.3, pp. 613~627, 1995.
- [11] D. L. Donoho, "Interpolating wavelet transform," *Preprint*, Stanford Univ., 1992.
- [12] S. Dubuc, "Interpolation through an iterative scheme", *J. Math. Anal. and App.*, vol.114, pp.185~204, 1986.
- [13] A. Harten, "Multiresolution representation of data: a general framework," *SIAM J. Num. Analysis*, vol.33, no.3, pp.1205-1256, 1996.

- [14] C. Herley, M. Vetterli, "Orthogonal time-varying filter banks and wavelet packets," *IEEE Trans. SP*, Vol. 42, No. 10, pp.2650-2663, October 1994.
- [15] C. Herley, Z. Xiong, K. Ramchandran and M. T. Orchard, "Joint Space-frequency Segmentation Using Balanced Wavelet Packets Trees for Least-cost Image Representation," *IEEE Trans. Image Processing*, vol. 6, pp. 1213-1230, September 1997.
- [16] D. K. Hoffman, N. Nayar, O. A. Sharafeddin, and D. J. Kouri, "Analytic banded approximation for the discretized free propagator," *J. Physical Chemistry*, vol.95, no.21, pp.8299-8305, 1991.
- [17] L. C. Jain, N. M. Blachman, and P. M. Chapell, "Interference suppression by biased nonlinearities," *IEEE Trans. IT*, vol.41, no.2, pp.496-507, 1995.
- [18] N. Jayant, J. Johnston, and R. Safranek, "Signal compression based on models of human perception", *IEEE Proceedings*, vol.81, no.10, pp.1385~1422, 1993.
- [19] I. M. Johnstone, B. W. Silverman, "Wavelet threshold estimators for data with correlated noise," *J. Royal Statistical Society, Series B*, vol. 59, pp.319-351, 1997.
- [20] J. Kovacevic, and M. Vetterli, "Perfect reconstruction filter banks with rational sampling factors," *IEEE Trans. SP*, Vol. 41, No. 6, pp.2047-2066, June 1993.
- [21] J. Kovacevic, W. Swelden, "Wavelet families of increasing order in arbitrary dimensions," Submitted to *IEEE Trans. Image Processing*, 1997.
- [22] A. F. Laine, S. Schuler, J. Fan and W. Huda, "Mammographic feature enhancement by multiscale analysis," *IEEE Trans. MI*, vol.13, pp.725-740, 1994.
- [23] S. Mallat, "A theory for multiresolution signal decomposition: the wavelet representation," *IEEE Trans. PAMI*, Vol.11, No.7, pp.674-693, July 1989.
- [24] Y. Meyer, *Wavelets Algorithms and Applications*, SIAM, Philadelphia 1993.
- [25] R. Nowak, D. Nowak, R. Baraniuk, and R. Hellman, "Wavelet Domain Filtering for Nuclear Medicine Imaging," *Proceedings of IEEE Medical Imaging Conference*, Anaheim CA, November 1996.
- [26] K. Ramchandran, M. Vetterli, "Best wavelet packet bases in a rate-distortion sense," *IEEE Trans. Image Processing*, Vol.2, No.2, pp.160-175, April 1993.

- [27] K. Ramchandran, Z. Xiong, K. Asai and M. Vetterli, "Adaptive transforms for image coding using spatially-varying wavelet packets," *IEEE Trans. Image Processing*, vol. 5, pp. 1197-1204, July 1996.
- [28] O. Rioul, M. Vetterli, "Wavelet and signal processing," *IEEE Signal Processing Magazine*, pp.14-38, October 1991.
- [29] N. Saito, G. Beylkin, "Multiscale representations using the auto-correlation functions of compactly supported wavelets," *IEEE Trans. Signal Processing*, Vol.41, no.12, pp.3584-3590, 1993.
- [30] M. J. Shensa, "The discrete wavelet transform: wedding the a trous and Mallat algorithms", *IEEE Trans. SP*, vol.40, no.10, pp.2464~2482, 1992.
- [31] Z. Shi, Z. Bao, "Group-normalized processing of complex wavelet packets," *Science in China (E)*, Vol.26, No.12, 1996.
- [32] Z. Shi, Z. Bao, "Group-normalized wavelet packet signal processing", *Wavelet Application IV, SPIE*, vol. 3078, pp.226~239, 1997.
- [33] Z. Shi, Z. Bao, "Fast image coding of interval interpolating wavelets," *Wavelet Application IV, SPIE*, vol. 3078, pp. 240-253, 1997.
- [34] Z. Shi, D. J. Kouri, G. W. Wei, and D. K. Hoffman, "Generalized symmetric interpolating wavelets," *Computer Phys. Comm.*, in press.
- [35] Z. Shi, G. W. Wei, D. J. Kouri, D. K. Hoffman, "Perceptual normalized subband image restoration," *IEEE Symposium on Time-frequency and Time-scale Analysis*, N.144, pp.469-472, Pittsburgh, Penn., Oct.6-9, 1998.
- [36] Z. Shi, G. W. Wei, D. J. Kouri, and D. K. Hoffman, "Visual group normalization using Gaussian-Lagrange distributed approximating functional wavelets," submitted to *IEEE SP Letter*, 1998.
- [37] W. Swelden, "The lifting scheme: a custom-design construction of biorthogonal wavelets," *Applied and Comp. Harmonic Analysis*, vol.3, no.2, pp.186~200, 1996.
- [38] T. D. Tran, R. Safranek, "A locally adaptive perceptual masking threshold model for image coding," *IEEE ICASSP*, pp.1882-1885, 1996.
- [39] M. Unser, A. Adroubi, and M. Eden, "The L_2 polynomial spline pyramid," *IEEE Trans. PAMI*, vol.15, no.4, pp.364-379, 1993.
- [40] P. Vaidyanathan, T.Chen, "Role of anti-causal inverse in multirate filter-banks—Part I: system-theoretic fundamentals," *IEEE Trans. SP*, Vol.43, No.5, pp.1090-1102, May 1995.

- [41] P. Vaidyanathan, T. Chen, "Role of anti-causal inverse in multirate filter-banks—Part II: the FIR case, factorizations, and biorthogonal lapped transforms," *IEEE Trans. SP*, Vol.43, No.5, pp.1103-1115, May 1995.
- [42] M. Vetterli, C. Herley, "Wavelet and filter banks: theory and design," *IEEE Trans. SP*, Vol. 40, No. 9, pp.2207-2232, September 1992.
- [43] J. D. Villasenor, B. Belzer, and J. Liao, "Wavelet filter evaluation for image processing," *IEEE Trans. IP*, vol.4, no.8, pp1053-1060, 1995.
- [44] A. B. Watson, G. Y. Yang, J. A. Solomon, and J. Villasenor, "Visibility of wavelet quantization noise," *IEEE Trans. Image Processing*, vol. 6, pp. 1164-1175, 1997.
- [45] G. W. Wei, D. S. Zhang, D. J. Kouri, and D. K. Hoffman, "Lagrange distributed approximating Functionals," *Physical Review Letters*, Vol. 79, No.5, pp. 775~779, 1997.
- [46] G. W. Wei, D. J. Kouri, and D. K. Hoffman, "Wavelets and distributed approximating functionals," submitted to *Phys. Rev. Letters*, 1998.
- [47] X.-G. Xia and Z. Zhang, "On sampling theorem, wavelets and wavelet transforms," *IEEE Trans. on Signal Processing*, Special Issue on Wavelets and Signal Processing, Dec. 1993.
- [48] Z. Xiong, K. Ramchandran and M. T. Orchard, "Space-frequency quantization for wavelet image coding," *IEEE Trans. Image Processing*, vol. 6, pp. 677-693, May 1997.
- [49] S. H. Zhang, Z. Bao, etc. "Target extraction from strong clutter background," *Tech. Rep.*, National Key Lab. of Radar Signal Processing, Xidian University, 1994.